Hydrogen in nanostructured vanadium-hydrogen systems

Shin-ichi Orimo
Faculty of Integrated Arts and Sciences, Hiroshima University, Higashi-Hiroshima 739-8521, Japan

Frank Kimmerle and Günter Majer
Max-Planck-Institut für Metallforschung, Heisenbergstrasse 1, D-70569 Stuttgart, Germany

(Received 6 June 2000; revised manuscript received 20 October 2000; published 13 February 2001)

Nanostructured vanadium-hydrides, β_2-VH_x, with typical grain sizes of 80 nm ($x=0.82$), 30 nm ($x=0.73$), and 10 nm ($x=0.67$) were prepared by mechanical milling under hydrogen atmosphere. The final grain size, about 10 nm, does not change any more with increasing milling time, and a homogeneous amorphous phase is not formed in this system, even after milling for 300 min. The hydrogen concentration in the grains x_G decreases with decreasing grain size from $x_G=0.82$ in 80-nm grains to 0.72 in 10-nm grains. This indicates a modification of the β_2-γ phase boundary in the V-H system with nanometer-scale grains. The hydrogen concentration in the intergrains, $x_{IG} \approx 0.5$–0.6, is smaller than in the grains, and was found to be nearly independent of the grain size. The hydrogen diffusivity has been studied by NMR measurements of the proton spin-lattice relaxation Γ_1. Generally, the measured Γ_1 consists of contributions that result from both hydrogen in the grains and in the intergrain regions. Due to the smaller spin-spin relaxation rate Γ_2 of the protons in the intergrain regions, their contribution to Γ_1 could be measured separately by the spin-echo technique. The relaxation data indicate that, at a given temperature, the hydrogen diffusivity in the intergrain regions is substantially higher than inside the grains. The frequency dependence of the dipolar contribution $\Gamma_{1,dip}$ reveals a distribution in the activation enthalpy for hydrogen in the intergrain regions. This distribution was found to be the broader the smaller the grain size. A change in the diffusion mechanisms, presumably arising from the $\beta_2-\delta$ phase transition, takes place at about 200 K. The exchange of hydrogen atoms between the grains and the intergrain regions occurs very slowly and is negligible on the time scale given by Γ_1.

DOI: 10.1103/PhysRevB.63.094307 PACS number(s): 66.30.−h, 81.20.−n, 81.40.−z, 76.60.Es

I. INTRODUCTION

The binary system VH_x has been extensively investigated over many years (see, e.g., Ref. 1). Particular attention has been given to the diffusion mechanisms as well as to the different kinds of ordered hydride phases.

A phase diagram of VH_x was reported by Maeland,[2] and then, a number of papers on the preparation and characterization of the hydride phases have been published.[3–16] Figure 1 shows one of the more recent phase diagrams by Pesch *et al.*[15] Around room temperature, the VH_x system is in a mixed α-β_1 phase for $x<0.5$. In the α phase the hydrogen atoms occupy randomly the tetrahedral sites (T sites) of the body-centered-cubic (bcc) host lattice, while in the β_1 phase octahedral sites (O_z sites) of the body-centered-tetragonal (bct) host lattice are occupied. The δ phase, a low-temperature phase, exhibits a specific hydrogen sublattice which resembles that of the β_1 phase. With increasing hydrogen concentration, from $x\approx 0.5$ to about 0.8, the β_1 phase transforms into the β_2 phase. The VH_x system is in a mixed β_2-γ phase for $x>0.8$. In the γ phase with $x=2$ the vanadium lattice has a face-centered-cubic (fcc) structure, where hydrogen atoms occupy the T sites.

In the β_1, β_2, and δ phases, the host lattice is tetragonally distorted with $c/a\approx 1.1$ due to the preferential occupation of the O_z sites by hydrogen (see, e.g., Refs. 1, 10, 13, and 17). These phases are composed of two kinds of (101) stacking planes of O_z sites, the so-called O_{z1} and O_{z2} sites. The stacking sequence is 121212, etc. for the β_1 phase, and 112112, etc. for the δ phase.[13] For the stoichiometric compositions, i.e., $VH_{0.5}$ for the β_1 phase and $VH_{0.67}$ for the δ phase, the O_{z1} sites are filled with hydrogen atoms and the O_{z2} sites are empty. In the hyperstoichiometric compositions of the β_1 and δ phases the O_{z2} sites are also partially filled. In the β_2 phase hydrogen occupies both O_{z1} and O_{z2} sites randomly.

The β_2-γ phase boundary was precisely determined to be at $x=0.82$ at room temperature by x-ray diffraction and NMR studies,[18] as also shown in Fig. 1. Although the value $x=0.82$ is lower than that in some VH_x phase diagrams,[15] it

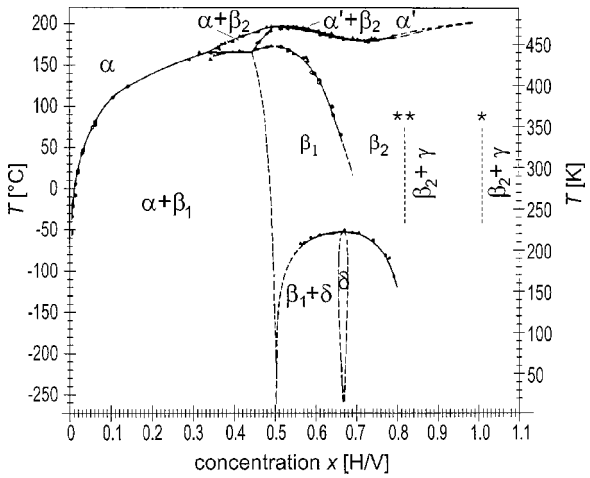

FIG. 1. Phase diagram of VH_x (from Ref. 15). In addition to the β_2-γ phase boundary reported by Pesch *et al.* (Ref. 15) (*), the results of Cantrell *et al.* (Ref.18) are also indicated (**).

is consistent with the phase boundary reported previously by Maeland[2] and Luo *et al.*[19]

An important feature of bulk VH_x is the high diffusivity of hydrogen in the α phase, even at low temperatures. Gorski-effect measurements revealed a diffusion coefficient of $D=5\times10^{-9}$ m^2 s^{-1} at room temperature in α-VH_x.[20,21] From the temperature dependence of D between about 140 and 570 K an activation enthalpy of $H=45$ meV has been deduced.[20,21] At higher hydrogen concentrations, Gorski-effect measurements are not possible because of the hydrogen embrittlement.

Nuclear magnetic resonance (NMR) offers unique capabilities to measure the diffusivity on powdered samples. The jump frequency of the hydrogen atoms can be deduced from the dipolar contribution $\Gamma_{1,dip}$ to the proton spin-lattice relaxation rate Γ_1. Pulsed-field-gradient (PFG) spin-echo NMR, on the other hand, permits measurement of the long-range diffusivity D.[22,23]

PFG measurements of the hydrogen diffusion in the α' phase of bulk VH_x have been performed by Kleiner and co-workers.[24] It has been found that the activation enthalpy H increases with increasing x from $H=87$ meV ($x=0.17$) to $H=132$ meV ($x=0.68$), resulting in a strong decrease in D. Proton relaxation rates and line shapes have been studied most intensively in the hydride phases of vanadium.[10,18,25–28] The complex dependence of Γ_1 on temperature and hydrogen concentration has been elaborated in order to deduce hydrogen diffusion parameters.[10,18,25,27,28] It has been found that the transition from the α phase to an ordered hydride phase results in a discontinuous drop in D by more than two orders of magnitude.[10] The activation enthalpies $H=230$ meV ($x=0.546$) and 240 meV ($x=0.622$) have been reported for hydrogen diffusion in the β_1 and/or β_2 phase of VH_x in the temperature range below room temperature. At higher temperatures, $H\approx300$–400 meV has been found for $0.486\leqslant x\leqslant0.736$.[10]

Up to now, all investigations on VH_x have been carried out on polycrystalline samples with rather large grain sizes typically in the micrometer-scale or bigger, or single-crystalline ones. In this case, the fraction of grain boundaries is almost negligible, and thus the hydriding properties of the whole material is dominated by that of the crystalline grains.

Samples with crystalline grains in the nanometer range,[29] so-called nanostructured (nanocrystalline) materials,[30] become increasingly important from the viewpoint of application as well as for basic research. Owing to the rather large volume fraction of grain boundaries many physical properties are fundamentally changed in a nanostructured system. The diffusion coefficient of hydrogen in the grain boundaries is a particularly important quantity in this context, which is difficult to measure.

The grain boundaries, as defined by the range of pronounced atomistic rearrangements of the metal atoms, will in the following be denoted as *intergrains*. Their thickness is typically between 0.5 and 1.5 nm. The hydrogen dynamics, however, may be affected in a somewhat wider range, which, in order to draw a distinction, will be denoted by *intergrain region*.

Specific changes of the hydriding properties in comparison to polycrystalline or single-crystalline materials have been reported for nanostructured materials, in both thermodynamical and diffusional aspects. The intergrains play an important role in the hydrogen uptake.[31–34] In the case of nanostructured PdH_x, for example, an increase in the hydrogen solubility has been observed, which results from an enhanced hydriding ability of the intergrains.[35–38] Another specific property is the promotion or retardation of the hydrogen diffusivity, which depends on the hydrogen concentration in the intergrains, as it has been extensively studied on NiH_x.[39–51] Models for different hydrogen diffusivities in the grains and intergrain regions were presented and compared with experimental results.[52–55]

In this work, nanostructured VH_x has been prepared by mechanical milling under hydrogen atmosphere. The (crystalline) structures and hydrogen concentrations both in the grains and intergrains of the nanostructured β_2-VH_x at the β_2-γ phase boundary have been studied. Furthermore, we report here the first studies of hydrogen diffusion in 80-nm $VH_{0.82}$, 30-nm $VH_{0.73}$, and 10-nm $VH_{0.67}$ by using nuclear magnetic resonance. The NMR data revealed differences in the hydrogen dynamics inside the grains and in the intergrain regions. The diffusion parameters obtained for hydrogen in the intergrain regions are compared with those for hydrogen in bulk VH_x.

II. EXPERIMENTAL DETAILS

A. Sample preparation

Pure vanadium (purity better than 99.5% with impurities of 410 ppm Al, 250 ppm Fe, 120 ppm Si, and 0.27 mass % O including surface oxygen) of about 10 μm in particle size was used as host sample. 1g of the host sample was placed together with 20 steel balls of 7 mm in diameter (mass ratio 1:30) in a steel vial. The vial, which was equipped with a connection valve for evacuation or introduction of hydrogen, was degassed for 720 minutes below 10^{-4} Pa. Subsequently, high-purity hydrogen (99.9999% purity) of 1.0 MPa was introduced. The mechanical milling was performed at room temperature by using a planetary milling apparatus (Fritsch P5) with 400 rpm for periods of up to 300 min.

Attention was paid to avoid impurity effects on the hydriding and structural properties of the samples as far as possible.[56,57] Therefore the material and shape of the vial were carefully selected, so as to minimize the contamination of the samples with elemental Fe during the milling process. In addition, the vial containing the sample was, as mentioned above, directly degassed prior to the milling. In order to reduce the oxidation of the sample, it was always handled in an argon glove box before and after the milling process.

The remaining hydrogen pressure after the milling was about 0.1 MPa, and the sample of about 1–10 μm in particle size was prepared without a significant increase of the impurities: 880 ppm Fe and 0.30 mass % O, including surface oxygen, even after milling for 60 min.

B. Sample analysis

The samples were characterized by x-ray diffraction (XRD), transmission electron microscopy (TEM), and thermal desorption mass spectroscopy (TDS).

The XRD measurements (Cu-K_α) were carried out by using a Siemens D5000 diffractometer to determine the phase transitions, and also by using a Rikaku RINT 2000 diffractometer to precisely analyze both the grain size and the lattice parameter from peak broadening and peak position, respectively.

The TDS measurements of hydrogen was carried out under a high vacuum using 10–20 mg of each sample and a heating rate of 5–10 K/min up to 773 K. The system was calibrated by analyzing a reference sample, and the accuracy of the obtained hydrogen concentration is within 5% of the quoted value.[58]

C. Nuclear-magnetic-resonance studies

Measurements of the proton spin-lattice relaxation rates Γ_1 were performed between 75 and 310 K at resonance frequencies of 10.5, 27.7, 67.7, and 139.4 MHz. The upper limit of 310 K was not exceeded in order to avoid structural relaxation and recrystallization of the nanostructured samples. Temperatures below room temperature were achieved by cooling with cold nitrogen/helium gas in a separate cryostat in the room-temperature bore of the superconducting magnet. The sample temperature was maintained by means of a digital PID controller combined with Ohmic heating and it was monitored with two calibrated Pt resistors. The maximum temperature drift during a measurement was ± 0.5 K and the absolute value of the temperature could be determined to an accuracy of ± 0.5 K. The NMR signals were observed with a home-built Fourier transform spectrometer using phase-alternating pulse schemes and quadrature detection. The spin-lattice relaxation rates were determined with an inversion-recovery pulse sequence ($180°$-τ_1-$90°$). Only at the lowest temperatures with $\Gamma_1 \ll 1\ \mathrm{s}^{-1}$, a saturation pulse train was used instead of the $180°$ pulse. The recovered magnetization was inspected for different waiting times τ_1 either by measuring the free induction decay (FID) after a delay time t_d or by measuring the spin echo following the pulse sequence [$(90°)$-τ_2-$180°$-τ_2]. The Γ_1 values were finally obtained by fitting single-exponential recovery curves to the magnetization. If a sample consists of several components with different spin-spin relaxation rates Γ_2 their contributions to the measured Γ_1 depend on the values of the delay time t_d or the spin-echo time $2\tau_2$, which were chosen in the experiment.

III. RESULTS AND DISCUSSION

A. Size and crystalline structure of the grains

Figure 2 shows the XRD profiles measured after mechanical milling under hydrogen atmosphere. The shift of the peak positions to slightly lower angles after 1 min suggests the formation of the α phase resulting from the hydrogen dissolution in the bcc host lattice. After the milling for 2 min, additional diffraction peaks appear, indicating the tetragonal distortion in part of the sample.

The single β phase (''β_2 phase'' in precise, as described later) was prepared already after 5 min milling at room temperature. This experimental fact is quite important from the viewpoint of appropriate sample preparation, because this preparation process results in much lower probabilities of oxygen solution into the sample. In conventional gas-phase hydrogenation, activation treatments at high temperatures (500–600 K) and high hydrogen pressures (≈ 3.0 MPa) are necessary for the hydrogenation, and therefore the oxygen on the surface easily solves into the samples.

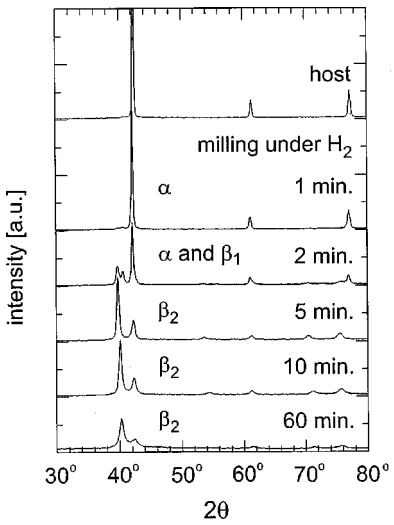

FIG. 2. X-ray diffraction profiles of host vanadium and nanostructured vanadium hydrides prepared by mechanical milling for 1, 2, 5, 10, and 60 min under hydrogen atmosphere.

The grain size of the β_2 phase decreases with further milling process after 5 min. Table I(a) gives the grain sizes obtained by the Scherrer method of the peak broadening. By using the Wilson method[59] we found that there is no detectable lattice strain in the samples, as reported previously for Mg_2Ni mechanically milled under hydrogen atmosphere.[56] The grain sizes of the samples correspond well to TEM observations. For example, the TEM image of the 60 min

TABLE I. Nanostructured vanadium hydrides, β_2-VH_x, prepared by mechanical milling for 5, 10, and 60 min under hydrogen atmosphere: (a) Average grain size obtained by the analysis of the peak broadening in the x-ray-diffraction profiles given in Fig. 2. (b) Lattice parameters a_0 and c_0 calulated from the peak position in the x-ray diffraction profiles given in Fig. 2, and resulting unit-cell volume ν_G. (c) Hydrogen concentration in the grains x_G calculated from the unit-cell volume. (d) Total hydrogen concentration x measured by thermal desorption mass spectroscopy.

Milling time (min)	5	10	60
(a) Average grain size (nm)	80	30	10
(b) Lattice parameters			
a_0 (nm)	0.3024	0.3031	0.3020
c_0 (nm)	0.3428	0.3386	0.3391
unit-cell volume ν_G (10^{-2} nm^3)	3.136	3.111	3.093
Hydrogen concentration			
(c) In the grains x_G	0.82	0.76	0.72
(d) Total concentration x	0.82	0.73	0.67

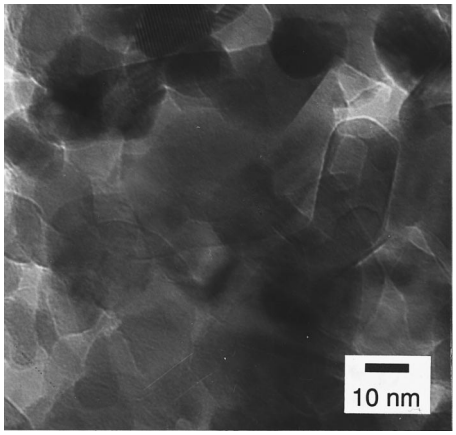

FIG. 3. Transmission electron microscopy image of VH_x ($x = 0.67$) prepared by mechanical milling for 60 min under hydrogen atmosphere.

milled sample, shown in Fig. 3, indicates that the typical grain size is of the order of 10-nm.

It should be noted that the sample with 10-nm grains is still in the crystalline state of the β_2 phase composed from both the grains and intergrains, not in the homogeneous amorphous state. The sample milled for 300 min is, as we confirmed, also in the crystalline state of the β_2 phase.

B. Hydrogen concentration in the grains

The lattice constants and unit-cell volumes obtained by the analysis of the peak positions are summarized in Table I(b). In addition, we estimated the hydrogen concentration in the grains, $x_G = H_{grain}/V_{grain}$, on the basis of the previously reported relationship between the hydrogen concentration and the unit-cell volume, ν_G, as follows from Ref. 18;

$$\nu_G(10^{-2}\ \text{nm}^3) = 2.7661 + 0.4532 \cdot x_G. \tag{1}$$

The results for x_G thus obtained are given in Table I(c).

In the sample with 80-nm grains, the obtained hydrogen concentration, $x_G = 0.82$, corresponds very well to the concentration at the conventional β_2-γ phase boundary, as reported by Cantrell *et al.*[18] for the polycrystalline sample. With decreasing the grain size, on the other hand, the hydrogen concentrations gradually shift to the smaller values; $x_G = 0.76$ and 0.72 in the samples with 30-nm and 10-nm grains, respectively. These results indicate the modification of the β_2-γ phase boundary in the V-H system with nanometer-scale grains.

The hydrogen concentrations estimated for the grains may correspond to those at the β_2-γ phase boundary, because the final hydrogen pressure after the milling is located just below the miscibility gap (plateau) pressure between the β_2 and γ phases at room temperature.[3] At present, however, the slope of the pressure-composition isotherms is not estimated for the samples with 30- and 10-nm grains, as it would be required for an exact determination of the shift of the β_2-γ phase boundary.

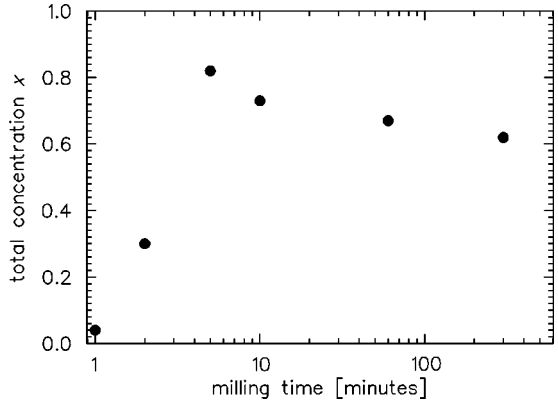

FIG. 4. Milling-time dependence of the total hydrogen concentration, $x = H_{total}/V_{total}$, determined by thermal desorption mass spectroscopy.

C. Total hydrogen concentration

The total hydrogen concentration, $x = H_{total}/V_{total}$, was precisely determined by TDS measurements. The milling-time dependence of x is given in Fig. 4. The values of x increase with increasing milling time, and reaches $x = 0.82$ after 5 min, i.e., in the sample with 80-nm grains. This hydrogen concentration is in excellent agreement with that in the grains x_G and also with the value at the β_2-γ phase boundary.[18] With decreasing grain size, however, the value of x decreases more strongly than x_G, as summarized in Table I(d). This result indicates that the hydrogen concentration in the intergrains, $x_{IG} = H_{intergrain}/V_{intergrain}$, is smaller than that in the grains x_G. A quantitative analysis of x_{IG} is described in the next section.

D. Volume fraction and hydrogen concentration in the intergrains

First we estimate the volume fraction of the intergrains, F, as follows:[29]

$$F = 3 \cdot I/C. \tag{2}$$

Here I denotes the width of the intergrains, which is defined by the range of pronounced atomistic rearrangements of the vanadium atoms, and C is the average grain size. It is reasonable to assume that I is about 1 nm. This results in the volume fraction F of less than 5%, about 10%, and about 30% in 80-nm $VH_{0.82}$, 30-nm $VH_{0.73}$, and 10-nm $VH_{0.67}$, respectively.

On the basis of these volume fractions, the hydrogen concentration in the intergrains x_{IG} is calculated by using the equation

$$x = (1 - F) \cdot x_G + F \cdot x_{IG}. \tag{3}$$

The calculated values are in the range of $x_{IG} = 0.5$–0.6 for both the samples with 30- and 10-nm grains. In the sample with 80-nm grains, the volume fraction of the intergrains is too small for a reasonable estimate of x_{IG}.

The smaller hydrogen concentration in the intergrains, which seems to be nearly independent of the grain size, must

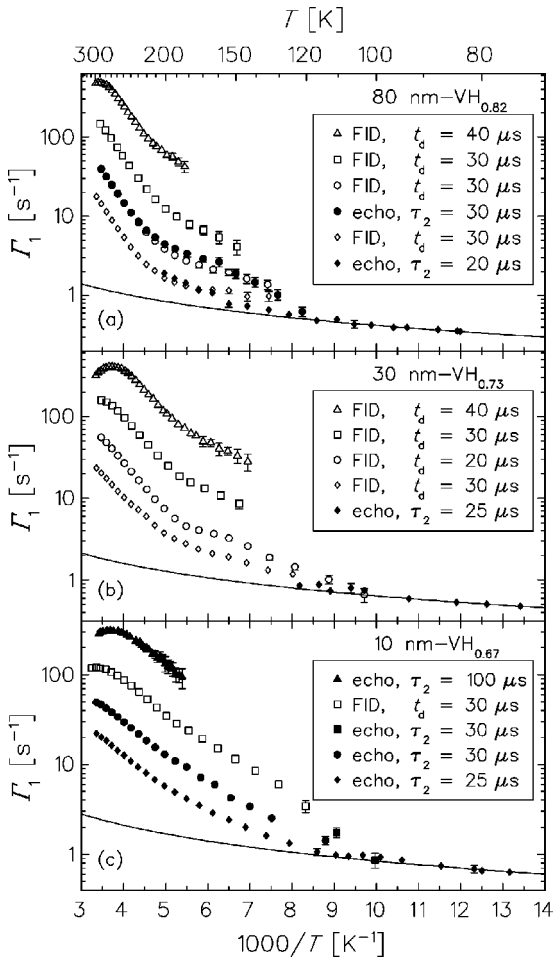

FIG. 5. Spin-lattice relaxation rate Γ_1 of hydrogen in the nanostructured vanadium hydrides (a) 80-nm $VH_{0.82}$, (b) 30-nm $VH_{0.73}$, and (c) 10-nm $VH_{0.67}$. The data were deduced from measurements of the free induction decay (FID: open symbols) or from the spin-echo experiments (echo: full symbols) with the indicated parameters t_d or τ_2. The solid lines represent the electronic contributions $\Gamma_{1,e}$. Measurements were performed at 10.5 MHz (triangles), 27.7 MHz (squares), 67.7 MHz (circles), and 139.4 MHz (diamonds).

be related to specific structural properties of the intergrains. In the intergrains, no long-range ordering of vanadium atoms for the preferential hydrogen occupations in the O_z site is expected. Moreover, the lattice deformation in the intergrains results in the formation only of tetrahedral coordination, as has been concluded from the atomic structures of the alloys prepared by mechanical milling.[60] Recent neutron-diffraction measurements[61] could, indeed, be interpreted in terms of *T*-site occupation of deuterium in the intergrains of the nanostructured β_2-VD_x.

E. Diffusion parameters of hydrogen

Figure 5 shows the spin-lattice relaxation rates Γ_1 of hydrogen in 80-nm $VH_{0.82}$, 30-nm $VH_{0.73}$, and 10-nm $VH_{0.67}$, as deduced either from the FID or from the spin-echo experiments. The data were taken at different frequencies $\omega/2\pi$ and with different operating parameters (t_d and τ_2). In a metal-hydride the proton spin-lattice relaxation rate Γ_1 is usually given by the sum of two contributions according to

$$\Gamma_1 = \Gamma_{1,e} + \Gamma_{1,dip}. \tag{4}$$

The electronic contribution $\Gamma_{1,e}$, resulting from the interaction between the magnetic moments of protons and conduction electrons, is well described by the relationship[62]

$$\Gamma_{1,e} = T/\kappa. \tag{5}$$

The Korringa constant κ depends on the density of electronic states $N(E_F)$ at the Fermi level according to $\kappa \propto N(E_F)^{-1/2}$. For all three samples κ has been determined by a fit of Eq. (5) to the data measured at $\omega/2\pi = 139.4$ MHz and at low temperatures, where the dipolar contribution is negligible. The obtained values are $\kappa = 238 \pm 1$ Ks, 157 ± 1 Ks, and 119 ± 2 Ks for the samples 80-nm $VH_{0.82}$, 30-nm $VH_{0.73}$, and 10-nm $VH_{0.67}$, respectively. The corresponding $\Gamma_{1,e}$ curves are shown in Fig. 5 as solid lines. These κ values indicate that the density of states of the conduction electrons at the Fermi level decreases with increasing hydrogen content. This conclusion is consistent with $\kappa = 110$ Ks determined for the not ball-milled system $VH_{0.59}$ by Hayashi *et al.*[27]

The dipolar spin-lattice relaxation rate $\Gamma_{1,dip}$ is due to the magnetic dipole-dipole interaction of a given proton with neighboring protons and with the host nuclei. The simplest approximation in order to obtain diffusion parameters is to analyze $\Gamma_{1,dip}$ in terms of a spectral density function that is a Lorentzian, as originally proposed for liquids by Bloembergen, Purcell, and Pound (BPP, Ref. 63). The spin-carrying hydrogen atoms remain at interstitial sites for the mean dwell time τ_d before they jump to neighboring sites in an infinitely short time. Thus the characteristic time for the dipolar interaction, the correlation time, is $\tau_c = \tau_d/2$ for the interaction between two hydrogen atoms and $\tau_c = \tau_d$ for the interaction between hydrogen and vanadium atoms. In the present systems, the contributions to $\Gamma_{1,dip}$ due to the hydrogen-hydrogen interaction is almost an order of magnitude smaller than that due to the hydrogen-vanadium interaction.

For the resonance frequency $\omega/2\pi$ the $\Gamma_{1,dip}$ maximum is observed at the temperature at which the condition $\omega\tau_d \approx 1$ is fulfilled. The asymptotic behavior of $\Gamma_{1,dip}$ is given by

$$\Gamma_{1,dip} \propto (\omega^2 \tau_d)^{-1} \tag{6}$$

for slow diffusion ($\omega\tau_d \gg 1$) and by

$$\Gamma_{1,dip} \propto \tau_d \tag{7}$$

for fast diffusion ($\omega\tau_d \ll 1$), provided that the diffusion process is determined by a single τ_d value at a given temperature. For a thermally activated diffusion process, τ_d is given by

$$\tau_d = \tau_{d,0} \exp(H/k_B T), \tag{8}$$

with the activation enthalpy *H*, and a temperature-independent prefactor $\tau_{d,0}$.

The diffusion-induced relaxation rate $\Gamma_{1,dip}$ was determined by subtracting $\Gamma_{1,e}$ from the measured Γ_1. It is evident from Fig. 5 that the present results cover mainly the low-temperature sides of the relaxation maxima ($\omega\tau_d \gg 1$). In a

TABLE II. Apparent activation enthalpies for hydrogen diffusion in the nanostructured vanadium hydrides 80-nm $VH_{0.82}$, 30-nm $VH_{0.73}$, and 10-nm $VH_{0.67}$. The H_{app} values were deduced from the low-temperature slopes of Arrhenius plots of $\Gamma_{1,dip}$, as calculated from the Γ_1 data shown in Fig. 5. H_{app}^{G} and H_{app}^{IG} are the corresponding values for hydrogen in the grains and intergrain regions. The results for 30-nm $VH_{0.73}$ are obtained from Fig. 8 and a similar analysis was done in the case of 80-nm $VH_{0.82}$. The H_{app}^{G} data are put in brackets, since these data are rather uncertain due to the influence from hydrogen in the intergrain regions. For 10-nm $VH_{0.67}$ no contribution from the grains could be observed, and H_{app}^{IG} is therefore identical to H_{app}. In the case of 80-nm $VH_{0.82}$ and 30-nm $VH_{0.73}$ the comparison of H_{app} with H_{app}^{IG} suggests that also in these samples the Γ_1 data of Fig. 5 are dominated by hydrogen in the intergrain regions.

	H_{app} [meV]		H_{app}^{G} [meV]	H_{app}^{IG} [meV]	
	120–200 K	200–300 K	200–300 K	120–200 K	200–300 K
80-nm $VH_{0.82}$	41±11	155±3	(172)		180±12
30-nm $VH_{0.73}$	48±3	121±4	(120)	59±9	134±4
10-nm $VH_{0.67}$	67±5	80±2		67±5	80±2

first approach, the activation enthalpies H were therefore calculated from the low-temperature slopes of the $\Gamma_{1,dip}$ data by using the relation

$$\Gamma_{1,dip} \propto \exp(-H/k_B T), \tag{9}$$

which follows from Eqs. (6) and (8). The slopes were determined simultaneously for all frequencies but separately for the temperature ranges $300>T>200$ K and $200>T>120$ K. The apparent activation enthalpies H_{app} obtained in this way are given in Table II. The different H_{app} values for temperatures above and below 200 K indicate a change in the diffusion mechanism. At first sight, this behavior reminds us of the mechanisms of quantum diffusion in the α phase of Nb and Ta.[64] But, the activation enthalpy in polycrystalline VH_x with a similar hydrogen content[10] as well as the average H value for hydrogen diffusion in the intergrain regions (see below) are both substantially higher than the H_{app} values of Table II and are too high to be interpreted in terms of tunneling processes. Thus we ascribe the change in the diffusion behavior at about 200 K to the phase transition from the β_2 to the δ phase.[15]

In both temperature ranges the overall temperature dependence of $\Gamma_{1,dip}$ in Fig. 5 is well described by Eq. (9) with the H_{app} values from Table II. However, in the case of 80-nm $VH_{0.82}$ and 30-nm $VH_{0.73}$, at a fixed T and ω the measured Γ_1 values depend slightly, but clearly, on the chosen pulse sequence and hereby on t_d or τ_2 (cf. Fig. 5). This can be understood quite naturally as due to different contributions to the NMR signal from hydrogen in the grains and the intergrain regions. The existence of different contributions to the NMR signal is evident from Fig. 6, which shows, as an example, the amplitude of the proton spin echo M measured on 30-nm $VH_{0.73}$ as a function of τ_2. These data were taken at $\omega/2\pi=139.4$ MHz and $T=268$ K. For a single-component system a plot of $\ln(M)$ versus τ_2 generally yields a straight line whose slope gives the spin-spin relaxation rate Γ_2. It is obvious from Fig. 6 that at least two components with different Γ_2 coexist in 30-nm $VH_{0.73}$, which explains the parameter dependence of the measured Γ_1 data (cf. Fig. 5).

Between 200 and 310 K, about 74% of the hydrogen in 30-nm $VH_{0.73}$ was detected in the component with the higher Γ_2 rate whereas 26% of hydrogen was observed in the component with the smaller Γ_2 rate. We ascribe the 74% component (with the higher Γ_2) to hydrogen in the grains and the 26% component (with the smaller Γ_2) to hydrogen in the intergrain regions. These fractions of hydrogen in the grains and in the intergrain regions yield a thickness of the intergrain regions of about 2.0–2.5 nm in 30-nm $VH_{0.73}$. Thus the intergrain regions, where the hydrogen diffusivity differs from that in the crystalline grains, have about twice the thickness of the intergrains seen by the transmission electron microscopy (0.5–1.5 nm). The assignment given above is further supported by the fact that, indeed, a smaller Γ_2^{IG} is expected for hydrogen in the intergrain regions compared to Γ_2^{G} in the grains: The smaller hydrogen density in the intergrain regions already results in a reduced Γ_2^{IG}, but this is only a weak effect, since the relaxation rates are dominated by the hydrogen-vanadium interaction. The main reduction of Γ_2^{IG} compared to Γ_2^{G} is caused by the higher mobility of

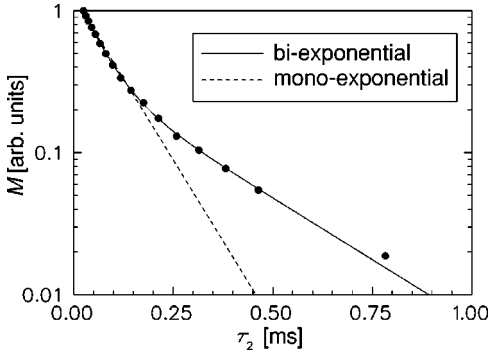

FIG. 6. Amplitude M of the spin echo following a $90°-\tau_2-180°-\tau_2$ sequence as a function of τ_2. This example shows measurements on 30-nm $VH_{0.73}$ at $\omega/2\pi=139.4$ MHz and $T=268$ K. The solid curve represents a fit for two components with different spin-spin relaxation rates Γ_2. The dashed line shows, for comparison, a recovery curve as expected for a single-component system.

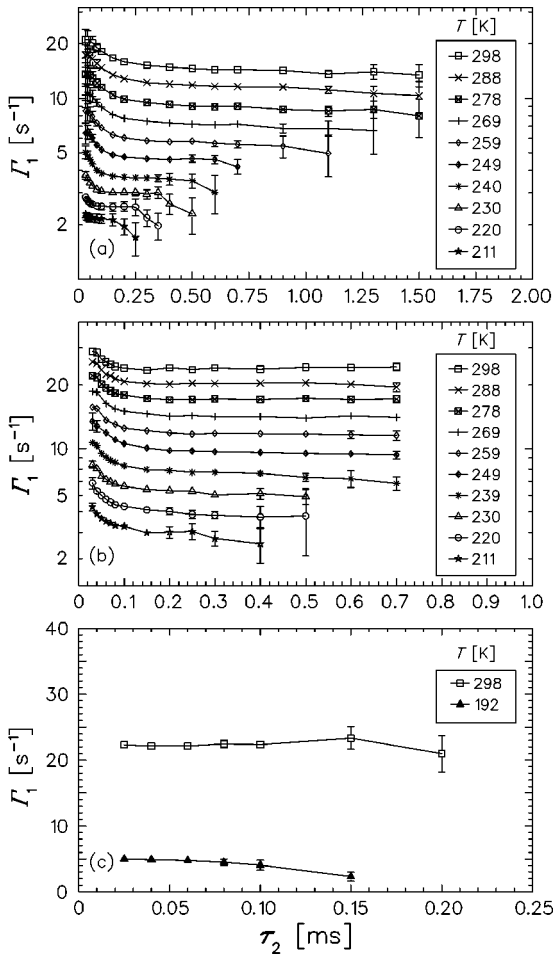

FIG. 7. Γ_1 data measured with the spin-echo detection method at 139.4 MHz in the nanostructured vanadium hydrides (a) 80-nm $VH_{0.82}$, (b) 30-nm $VH_{0.73}$, and (c) 10-nm $VH_{0.67}$. The data were taken at different temperatures T as a function of τ_2. Note the different scales of the axes.

hydrogen in the intergrain regions (see below). In the entire temperature range from 200 to 310 K, the ratio of Γ_2^G to Γ_2^{IG} was found to be approximately 4.

In order to study the hydrogen diffusion in the grains and intergrain regions separately, Γ_1 has been measured with the spin-echo detection method as a function of τ_2. The τ_2 values have been varied systematically between the lower limit, given by the dead time of the amplifiers, and the upper limit, given by the decrease in the signal-to-noise ratio. Figure 7 shows for all three samples the Γ_1 data taken at different temperatures and at 139.4 MHz. The observed τ_2 dependence of Γ_1 permits analysis of the relaxation rates of hydrogen in both the grains and the intergrain regions in the way described immediately below.

In the samples 80-nm $VH_{0.82}$ and 30-nm $VH_{0.73}$ the measured Γ_1 first decreases and then reaches a plateau value as τ_2 is increased. With increasing τ_2, the NMR signal from the protons inside the grains disappears first, because of their higher spin-spin relaxation rate Γ_2^G compared to Γ_2^{IG}. The plateau values can therefore be directly interpreted as Γ_1^{IG}, the spin-lattice relaxation rate of hydrogen in the intergrain regions. The spin-lattice relaxation rate of hydrogen in the grains Γ_1^G cannot be determined separately, since in the total NMR signal always a component due to hydrogen in the intergrain regions is superimposed. The Γ_1 values of Figs. 7(a) and 7(b) measured with the shortest τ_2, which are greater than Γ_1^{IG}, represent $\Gamma_1^{G,min}$, a lower limit for the spin-lattice relaxation rate of hydrogen in the grains.

At first sight it is surprising that at temperatures below the relaxation maximum ($\omega\tau_d \gg 1$) Γ_1^{IG} was found to be smaller than Γ_1^G, although the hydrogen mobility is higher in the intergrain regions than inside the grains. If the relaxation strengths (the so-called second moments M_2) of the two hydrogen spin systems differ only little from one another, Eq. (6) predicts the opposite behavior for diffusion processes which are determined by *single* τ_d values at a given temperature. Thus one may think of a smaller M_2 in the intergrain regions due to the smaller hydrogen content and/or the hydrogen occupation of different interstitial sites. But, M_2 is dominated by the hydrogen-vanadium interaction and the smaller hydrogen content reduces M_2 only slightly. Moreover, if one assumes that in the intergrain regions T sites are occupied by hydrogen atoms,[60,61] M_2 would be even 20% greater than for pure O-sites occupation. On the other hand, a reduction in the maximum relaxation rate and a broadening of the width of the $\Gamma_{1,dip}$ peak is expected in a system in which a distribution of τ_d values exists.[23] The analysis of the Γ_1 data measured on 10-nm $VH_{0.67}$ indicates that there is indeed a broad distribution of the activation enthalpies H and thus of the τ_d values of hydrogen diffusion in the intergrain regions (see below). Thus we conclude that the smaller Γ_1^{IG} compared to Γ_1^G is due to the distribution of the H values in the intergrain regions.

The fact that the measured values of Γ_1 depend on τ_2 indicates that during the experiments no strong exchange of hydrogen atoms between the grains and the intergrain regions takes place. The exchange rate must be substantially smaller than the Γ_1 values, which are typically in the range of $1-10\ s^{-1}$. In the case of a considerably higher exchange rate, the measurements would yield an average Γ_1 value, and no independent contributions from grains and intergrain regions to the NMR signal could be isolated.

As can be seen in Fig. 7(c), in the case of 10-nm $VH_{0.67}$ the measured Γ_1 is independent of τ_2 within the experimental accuracy. Only the measurement at 192 K reveals for the longest τ_2 a smaller Γ_1 value, which, however, may be related to hydrogen trapping (see below). But, for short τ_2 there is no change in Γ_1, indicating that the contribution of hydrogen in the grains is no longer observable in this sample produced with the longest milling time. Obviously, even the shortest τ_2 is too long compared to $(\Gamma_2^G)^{-1}$. This may result from a general increase in the spin-spin relaxation rates with decreasing grain size. Moreover, the sample 10-nm $VH_{0.67}$ has the smallest volume fraction of the grains. From these results it follows that the Γ_1 rates shown in Fig. 5(c) originate solely from hydrogen in the intergrains, independently of the experimental parameters (t_d or τ_2). Therefore no further information can be obtained by systematic studies of the τ_2 dependence of Γ_1 on the 10-nm $VH_{0.67}$ sample using the

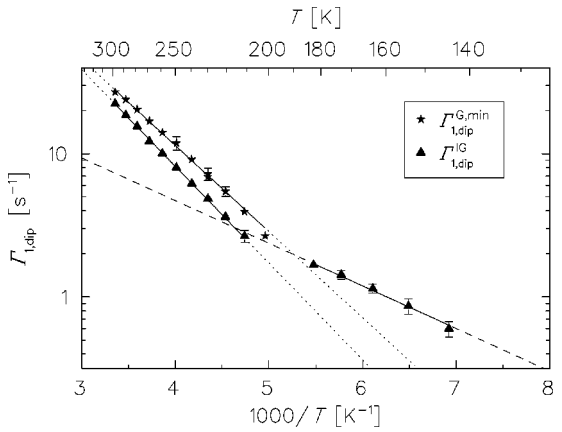

FIG. 8. Contributions of hydrogen in the grains and intergrain regions to the dipolar spin-lattice relaxation rate in 30-nm $VH_{0.73}$, as deduced from the Γ_1 data of Fig. 7(b). Γ_1^{IG} originates from hydrogen in the intergrains only, whereas $\Gamma_1^{G,min}$ represents a lower limit for hydrogen in the grains.

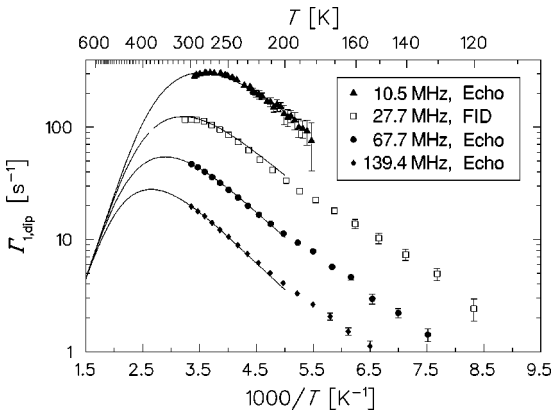

FIG. 9. Frequency dependence of $\Gamma_{1,dip}$ for hydrogen in 10-nm $VH_{0.67}$. The solid curves are obtained by a simultaneous fit of the BPP model to the data measured at different frequencies under the assumption of a Gaussian distribution of the activation enthalpy H. The fitting was done in the temperature range of the β_2 phase ($T \geqslant 200$ K) and it revealed the parameters $H_{average} = 239 \pm 6$ meV and $\Delta H = 53 \pm 4$ meV.

spin-echo detection method and thus these have been performed at two temperatures only.

From Fig. 7(a) it is evident that for $T \leqslant 249$ K, Γ_1 in 80-nm $VH_{0.82}$ drops down from a plateau value reached for long τ_2 to even lower rates Γ_1 at the longest τ_2. In the case of 30-nm $VH_{0.73}$ a similar behavior has been found below about 200 K, but, for clarity, this temperature range is not shown in Fig. 7(b). This indicates that a third contribution to Γ_1 exists, which can only be observed if the condition $\tau_2^{-1} \ll \Gamma_2^G, \Gamma_2^{IG}$ is fulfilled. In this τ_2 range the regular contributions to the NMR signal of hydrogen in grains and intergrain regions are negligible. This third contribution must be related to a small number of hydrogen atoms trapped at impurities. As typical for ball-milled systems, a small impurity content could not be avoided in the present samples. If one assumes that the trapped hydrogen atoms are quite immobile, i.e., their mean dwell time τ_d is increased, a reduction in $\Gamma_{1,dip}$ follows directly from Eq. (6). But, in this case it remains to be elucidated, why Γ_2 of the trapped hydrogen atoms appears to be smaller than that of the mobile hydrogen atoms. Therefore it seems to be more likely that the data have to be interpreted in terms of a very fast localized motion of the trapped hydrogen atoms, resulting in very short τ_d values. This would explain the reduction in $\Gamma_{1,dip}$ as well [cf. Eq. (7)], and, besides that, the comparably small Γ_2 of these trapped hydrogens could be easily understood.

In order to deduce diffusion parameters separately for hydrogen in grains and intergrain regions the temperature dependences of the corresponding dipolar relaxation rates, $\Gamma_{1,dip}^G$ and $\Gamma_{1,dip}^{IG}$, have to be considered. As outlined above, the present data yield values for Γ_1^{IG}, whereas only lower limits for Γ_1^G have been obtained. Moreover, it cannot be decided whether the electronic contributions $\Gamma_{1,e}$ differ significantly for hydrogen in grains and intergrain regions. But, on the other hand, the uncertainty in $\Gamma_{1,e}$ has only little effect on the activation enthalpies deduced from $\Gamma_{1,dip}$. Therefore, as a good approximation, the Korringa rates $\Gamma_{1,e}$ determined above have been subtracted from both $\Gamma_1^{G,min}$ and Γ_1^{IG} to calculate the dipolar contributions $\Gamma_{1,dip}^{G,min}$ and $\Gamma_{1,dip}^{IG}$. As an example, the $\Gamma_{1,dip}^{G,min}$ and $\Gamma_{1,dip}^{IG}$ values obtained in this way for 30-nm $VH_{0.73}$ are shown in Fig. 8. The $\Gamma_{1,dip}^{IG}$ data in the temperature range $144 \leqslant T \leqslant$ 183 K were deduced from τ_2 dependent measurements of Γ_1 not shown in Fig. 7(b). In this temperature range, no information on Γ_1^G could be obtained since Γ_2^G was too high. Similar results have been obtained in the case of 80-nm $VH_{0.82}$. The Arrhenius plot of Fig. 8 permits deduction of the apparent activation enthalpies, H_{app}^G and H_{app}^{IG}, for hydrogen in the grains and intergrains separately, by fitting Eq. (9) to the data. The different slopes below and above 200 K indicate again the phase transition from the β_2 to the δ phase. The obtained values of H_{app}^G and H_{app}^{IG} are included in Table II. The H_{app}^G data represent only rough estimates because of the contributions from hydrogen in the intergrain regions.

The system 10-nm $VH_{0.67}$ has the advantage that only one contribution to Γ_1, namely Γ_1^{IG}, has been observed. Therefore this system provides the opportunity to analyze directly the frequency dependence of $\Gamma_{1,dip}^{IG}$, which is obtained from Γ_1^{IG} in Fig. 5(c) by subtracting the electronic contribution $\Gamma_{1,e}$. Figure 9 shows an Arrhenius plot of $\Gamma_{1,dip}^{IG}$ obtained on 10-nm $VH_{0.67}$ at different resonance frequencies. On the low-temperature side of the relaxation maximum the observed frequency dependence of $\Gamma_{1,dip}^{IG}$ is significantly weaker than $\Gamma_{1,dip} \propto \omega^{-2}$ [cf. Eq. (6)], as predicted for a system with a single τ_d value. This may indicate a distribution of τ_d values. A reasonable approach is to use Eq. (8) and to average over a distribution of activation enthalpies H. The dipolar relaxation rate can than be written as[23]

$$\Gamma_{1,dip} = \int_0^\infty \Gamma_{1,dip}(H) G(H) \mathrm{d}H, \tag{10}$$

where $G(H)$ denotes the normalized distribution function.

The solid curves in Fig. 9 represent a simultaneous fit of Eq. (10) to all $\Gamma_{1,dip}^{IG}$ data above 200 K, using the BPP model for $\Gamma_{1,dip}(H)$ and a Gaussian distribution function $G(H)$

$\propto \exp[-(H_{\text{average}}-H)^2/2(\Delta H)^2]$. The obtained diffusion parameters are $H_{\text{average}}=239\pm 6$ meV and $\Delta H=53\pm 4$ meV. It should be stressed that these parameters describe both the temperature and the frequency dependence of $\Gamma_{1,\text{dip}}^{\text{IG}}$. Such a distribution of activation enthalpies is, indeed, expected for disordered structures like the intergrain regions of nanostructured samples. In spite of the rather large distribution width ΔH, single-exponential recovery curves were observed in the Γ_1 measurements on 10-nm $VH_{0.67}$, justifying the use of Eq. (10). This indicates a hydrogen hopping frequency $\nu^{\text{IG}} \gg \Gamma_{1,\text{dip}}^{\text{IG}}$. The value of H_{average} is in good agreement with the activation enthalpy $H=240$ meV reported for hydrogen diffusion in polycrystalline VH_x with a similar hydrogen content of $x=0.62$.[10] This suggests that the structural disorder in the intergrain regions results in a distribution of the barrier heights, but the average value H_{average} remains about the same as in the polycrystal. It is not yet understood, however, why the apparent activation enthalpies estimated for hydrogen in the grains $H_{\text{app}}^{\text{G}}$ (cf. Table II) deviate significantly from $H=240$ meV for a polycrystalline system. The value $H=240$ meV (Ref. 10) and a prefactor of $\tau_{\text{d},0}^{-1}\approx 10^{13}\ \text{s}^{-1}$, which is compatible with inelastic neutron-scattering experiments[65] and with the positions of the $\Gamma_{1,\text{dip}}$ maxima, yields a hydrogen hopping frequency at room temperature of ν^{G} (300 K) $\approx 1\times 10^9\ \text{s}^{-1}$. Using the same prefactor but the Gaussian distribution function for the activation enthalpies with $H_{\text{average}}=239$ meV and $\Delta H=53$ meV gives ν^{IG}(300 K) $\approx 8\times 10^9\ \text{s}^{-1}$. The distribution of H in the intergrain regions implies the existence of diffusion paths with reduced barrier height, which explains the higher diffusivity compared to that inside the crystalline grains. Moreover, the smaller hydrogen concentration in the intergrain regions should result in a higher prefactor $\tau_{\text{d},0}^{-1}$, due to a reduced blocking of occupied sites. If one takes this into account, the difference between the hydrogen diffusivities in the grains and intergrain regions is even bigger. The faster hydrogen diffusion in the intergrain regions is the main reason for the smaller Γ_2^{IG} values compared to Γ_2^{G}. The apparent activation enthalpies $H_{\text{app}}^{\text{IG}}$, which are given in Table II, correspond to the low-energy tails of the distribution functions. The fact that $H_{\text{app}}^{\text{IG}}$ is the smaller the longer the sample has been ball milled indicates an increase in the distribution width with decreasing grain size.

IV. SUMMARY AND CONCLUSIONS

Nanostructured β_2-VH_x $(0.67\leqslant x\leqslant 0.82)$ with various grain sizes was prepared by mechanical milling under hydrogen atmosphere. The single β_2 phase was prepared already after 5 min at room temperature. The crystalline structure of β_2 phase is retained, even in the sample with a typical grain size of 10 nm. The hydrogen concentration in the grains x_{G} decreases with decreasing grain sizes from $x_{\text{G}}=0.82$ with 80 nm to $x_{\text{G}}=0.72$ with 10 nm grains, because of the modification of the β_2-γ phase boundary in the V-H system with nanometer-scale grains. The hydrogen concentration in the intergrains $x_{\text{IG}}\approx 0.5-0.6$ is smaller than in the grains and appears to be nearly independent of the grain size.

The diffusivities of hydrogen in the nanostructured vanadium hydrides 80-nm $VH_{0.82}$, 30-nm $VH_{0.73}$, and 10-nm $VH_{0.67}$ were systematically investigated by NMR measurements. The use of a spin-echo sequence for signal detection enabled us to determine the spin-lattice relaxation rate of hydrogen in the intergrain regions Γ_1^{IG} independently of the contribution from the grains. The frequency and temperature dependence of the dipolar contribution $\Gamma_{1,\text{dip}}^{\text{IG}}$ showed conclusively that the hydrogen diffusion in the intergrain regions is governed by a distribution of activation enthalpies. In the case of 10-nm $VH_{0.67}$ the data above 200 K are well represented by a Gaussian distribution function with $H_{\text{average}}=239\pm 6$ meV and $\Delta H=53\pm 4$ meV. The distribution width, which is related to the structural disorder in the intergrain regions, was found to increase with decreasing grain size. The present diffusion parameters yield at the same given temperature a higher diffusivity in the intergrain regions than inside the crystalline grains. A similar increase in the diffusion coefficient has been reported previously, for example for hydrogen above a certain coverage in the intergrains of nanostructured nickel.[50] Although the hydrogen diffusivity in the intergrain regions is rather high, the exchange of hydrogen between grains and intergrain regions is negligible on the time scale of the Γ_1 measurements. Furthermore, the present diffusion studies reveal a change in the diffusion mechanisms at about 200 K, which may be ascribed to the phase transition from the β_2 to the δ phase.

ACKNOWLEDGMENTS

We thank Associated Professor H. Era for the TEM observations. The assistance of Dr. H. Reule in the TDS measurements and of Mr. E. Tanabe in the XRD measurements is appreciated. Also we are grateful to Professor H. Fujii, Professor Y. Fukai, and Dr. S. Hayashi for valuable discussion. One of the authors (S.O.) acknowledges support from the Alexander von Humboldt Foundation and from the Japanese Ministry of Education.

[1] T. Schober and H. Wenzl, in *Hydrogen in Metals II*, edited by G. Alefeld and J. Völkl (Springer, Berlin, 1978), p. 11.

[2] A. J. Maeland, J. Phys. Chem. **68**, 2197 (1964).

[3] J. J. Reilly and R. H. Wiswall, Jr., Inorg. Chem. **9**, 1678 (1970).

[4] D. G. Westlake, S. T. Ockers, and W. R. Grey, Metall. Trans. **1**, 1361 (1970).

[5] D. G. Westlake, S. T. Ockers, M. H. Müller, and K. D. Anderson, Metall. Trans. **3**, 1709 (1972).

[6] J. Wanagel, S. L. Sass, and B. W. Batterman, Phys. Status Solidi A **10**, 49 (1972); **11**, 767 (1972).

[7] H. Asano and M. Hirabayashi, Phys. Status Solidi A **16**, 69 (1973).

[8] R. R. Arons, H. G. Bohn, and H. Lütgemeier, J. Phys. Chem. Solids **35**, 207 (1974).
[9] H. Asano, Y. Abe, and M. Hirabayashi, Acta Metall. **24**, 95 (1976).
[10] Y. Fukai and S. Kazama, Acta Metall. **25**, 59 (1977).
[11] T. Schober and A. Carl, Phys. Status Solidi A **43**, 443 (1977).
[12] T. Schober, Scr. Metall. **12**, 549 (1978).
[13] H. Asano and M. Hirabayashi, Z. Phys. Chem. (Munich) **114**, 1 (1979).
[14] T. Schober and W. Pesch, Z. Phys. Chem. (Munich) **114**, 21 (1979).
[15] W. Pesch, T. Schober, and H. Wenzl, Scr. Metall. **16**, 307 (1982).
[16] T. Schober, Solid State Phenom. **49-50**, 357 (1996).
[17] H. Sugimoto, J. Phys. Soc. Jpn. **53**, 2592 (1984).
[18] J. S. Cantrell, R. C. Bowman, Jr., A. Attalla, and R. W. Baker, Z. Phys. Chem. (Munich) **181**, 83 (1993).
[19] W. Luo, J. D. Clewley, and T. B. Flanagan, J. Chem. Phys. **93**, 6710 (1990).
[20] J. Völkl and G. Alefeld, in *Hydrogen in Metals I*, edited by G. Alefeld and J. Völkl (Springer, Berlin, 1978), p. 321.
[21] Zh. Qi, J. Völkl, R. Lässer, and H. Wenzl, J. Phys. F: Met. Phys. **13**, 2053 (1983).
[22] R. M. Cotts, in *Hydrogen in Metals I*, edited by G. Alefeld and J. Völkl (Springer, Berlin, 1978), p. 227.
[23] R. G. Barnes, in *Hydrogen in Metals III*, edited by H. Wipf (Springer, Berlin, 1977), p. 93.
[24] J. E. Kleiner, E. H. Sevilla, and R. M. Cotts, Phys. Rev. B **33**, 6662 (1986).
[25] S. Kazama and Y. Fukai, Solid State Commun. **17**, 1039 (1975).
[26] S. Kazama and Y. Fukai, J. Phys. Soc. Jpn. **42**, 119 (1977).
[27] S. Hayashi, K. Hayamizu, and O. Yamamoto, J. Chem. Phys. **76**, 4392 (1982).
[28] R. C. Bowman, Jr., A. Attalla, and B. D. Craft, Scr. Metall. **17**, 937 (1983).
[29] T. Mütschele and R. Kirchheim, Scr. Metall. **21**, 135 (1987); **21**, 1101 (1987).
[30] R. Birringer, H. Gleiter, H.-P. Klein, and P. Marquardt, Phys. Lett. **102A**, 365 (1984).
[31] X. Zhu, R. Birringer, U. Herr, and H. Gleiter, Phys. Rev. B **35**, 9085 (1987).
[32] K. Lu, R. Lück, and B. Predel, Acta Metall. Mater. **42**, 2303 (1994).
[33] R. W. Siegel, Phys. Today **46** (10), 64 (1993).
[34] H. Gleiter, Z. Metallkd. **86**, 78 (1995).
[35] R. Kirchheim, T. Mütschele, W. Kieninger, H. Gleiter, R. Birringer, and T. D. Koblé, Mater. Sci. Eng. **99**, 457 (1988).
[36] J. A. Eastman, L. J. Thompson, and B.J. Kestel, Phys. Rev. B **48**, 84 (1993).
[37] P. G. Sanders, J. R. Weertman, J. G. Barker, and R. W. Siegel, Scr. Metall. **29**, 91 (1993).
[38] R. J. Wolf, M. W. Lee, and J. R. Ray, Phys. Rev. Lett. **73**, 557 (1994).
[39] T. Tsuru and R. M. Latansion, Scr. Metall. **16**, 575 (1982).
[40] D. H. Lassila and H. K. Birnbaum, Acta Metall. **34**, 1237 (1986).
[41] H. K. Birnbaum, B. Ladna, and A. Kimura, J. Phys. Colloq. **49**, C5-397 (1988).
[42] J. Yao and J. R. Cahoon, Scr. Metall. **22**, 1817 (1988).
[43] A. Kimura and H. K. Birnbaum, Acta Metall. **36**, 757 (1988).
[44] G. Palumbo, D. M. Doyle, A. M. El-Sherik, U. Erb, and K. T. Aust, Scr. Metall. Mater. **25**, 679 (1991).
[45] T. M. Harris and R. M. Latanision, Metall. Trans. A **22**, 351 (1991).
[46] J. Yao and J. R. Cahoon, Acta Metall. Mater. **39**, 111 (1991); **39**, 119 (1991).
[47] D. R. Arantes, X. Y. Huang, C. Marte, and R. Kirchheim, Defect Diffus. Forum **95-98**, 347 (1993).
[48] D. R. Arantes, X. Y. Huang, C. Marte, and R. Kirchheim, Acta Metall. Mater. **41**, 3215 (1993).
[49] R. Kirchheim, I. Kownacka, and S. M. Filipek, Scr. Metall. Mater. **28**, 1229 (1993).
[50] C. Marte and R. Kirchheim, Scr. Mater. **37**, 1171 (1997).
[51] J. Yao and S. A. Meguid, Int. J. Hydrogen Energy **22**, 1021 (1997).
[52] G. M. Pressouyre, Metall. Trans. A **10**, 1571 (1979).
[53] C. N. Park, J. Y. Lee, and G. W. Hong, J. Mater. Sci. Lett. **2**, 475 (1983).
[54] M. Hirscher, S. Zimmer, and H. Kronmüller, Z. Phys. Chem. (Munich) **183**, 51 (1994).
[55] M. Hirscher, J. Mössinger, and H. Kronmüller, J. Alloys Compd. **231**, 267 (1995).
[56] S. Orimo, H. Fujii, and K. Ideka, Acta Mater. **45**, 331 (1997).
[57] S. Orimo and H. Fujii, Intermetallics **6**, 185 (1998).
[58] H. Reule, Ph.D. thesis, University of Stuttgart, 1999.
[59] H.P. Klug and L.E. Alexander, *X-ray Diffraction Procedures for Polycrystalline and Amorphous Materials*, 2nd ed. (Wiley-Interscience Publication, New York, 1974), p. 618.
[60] T. Fukunaga, Physica B **213-214**, 518 (1995).
[61] K. Ito, T. Fukunaga *et al.* (unpublished).
[62] J. Korringa, Physica (Amsterdam) **16**, 601 (1950).
[63] N. Bloembergen, E. M. Purcell, and R. V. Pound, Physica (Amsterdam) **73**, 679 (1948).
[64] R. Messer, A. Blessing, S. Dais, D. Höpfel, G. Majer, C. Schmidt, A. Seeger, W. Zag, and R. Lässer, Z. Phys. Chem., Neue Folge Suppl.-H. **2**, 61 (1986).
[65] R. Hempelmann, D. Richter, and D. L. Price, Phys. Rev. Lett. **58**, 1016 (1987).